All-Solid-State Dye-Sensitized Solar Cells with Alkyloxy-Imidazolium Iodide Ionic Polymer/SiO₂ Nanocomposite Electrolyte and Triphenylamine-Based Organic Dyes

Jifu Shi, Ling Wang, Yanliang Liang, Shengjie Peng, Fangyi Cheng, and Jun Chen*

Institute of New Energy Material Chemistry and Key Laboratory of Advanced Micro/Nanomaterials and Batteries/Cells (Ministry of Education), Chemistry College, Nankai University, Tianjin 300071, People's Republic of China

Received: January 2, 2010

We report on all-solid-state dye-sensitized solar cells with alkyloxy-imidazolium iodide ionic polymer/SiO₂ nanocomposite electrolyte and triphenylamine-based metal-free organic dyes (TC15). By optimizing the content of I₂, 1,2-dimethyl-3-propylimidazolium iodide, and SiO₂ nanoparticles in the electrolyte, considerable ionic conductivity of 0.151 mS cm⁻¹ is achieved due to the formation of high-efficiency electron exchange tunnels. The electrolyte is further characterized by differential scanning calorimetry and scanning electron microscopy (SEM). The result of differential scanning calorimetry shows that the melting temperature of the electrolyte is 120 °C. The SEM analysis reveals a favorable interfacial contact between the electrolyte and the TiO₂. The all-solid-state solar cells with the as-prepared alkyloxy-imidazolium iodide ionic polymer/SiO₂ nanocomposite electrolyte and triphenylamine-based metal-free organic dyes attains high energy conversion efficiency of 2.70% and 4.12% under the illumination intensities of 100 and 10 mW cm⁻², respectively. This study should shed light on the development of all-solid-state dye-sensitized solar cells with nanocomposite ionic polymer electrolyte and metal-free organic dyes.

Introduction

Dye-sensitized solar cells (DSCs) have been attracting widespread scientific and technological interest and are regarded as an alternative to traditional photovoltaic devices due to their potential advantages of high efficiency (η) and low cost.[1] In the DSCs, both the electrolytes and the dyes play important roles in the determination of the energy-conversion efficiency and long-term stability.[2,3] At present, the organic solvent-based liquid-state electrolytes are usually used, which result in practical limitations of sealing and long-term operation at higher temperatures.[2] The quasi-solid-state DSCs using the gel electrolytes can alleviate these problems to some extent.[3] However, this approach still retains a significant volume of volatile liquid encapsulated in the gel pores, resulting in a large increase in vapor pressure as the temperature is raised.[4] It is thus that several attempts have been made to develop all-solid-state electrolytes such as p-type inorganic semiconductors (CuI, CuSCN etc.),[5,6] organic hole-transport materials (such as triarylamine and polythiophene-based derivatives),[7–9] and polymeric materials incorporating triiodide/iodide and/or inorganic nanoparticles.[4,10,11] Among them, the nanocomposite polymer electrolytes exhibited considerable photovoltaic performance due to the favorable ionic conductivity (σ), mechanical stability, and interfacial contact between the electrolyte and the TiO₂ film.[10,11]

Recently, imidazolium iodide-based room temperature ionic liquids (RTILs) have been applied in DSCs because of their outstanding stability and high ionic conductivity.[12] However, they are still a type of liquid material and rigorous sealing is necessary for this type of DSCs. On one hand, if the imidazolium iodide salts can be solidified through polymerization, the all-solid-state electrolyte prepared by this ionic polymer will possess advantages of both RTILs and polymer electrolyte. The property of this electrolyte can be further improved by the nanocomposite

method. However, to the best of our knowledge, this type of imidazolium iodide-based all-solid-state nanocomposite ionic polymer electrolyte for DSCs has been seldom reported. On the other hand, we have synthesized an alkyloxy-imidazolium iodide-based ionic polymer (AIIP), in which the imidazolium iodide is contained in the polymer chain, and successfully applied it in the quasi-solid-state DSCs,[13] indicating that the properties of AIIP can satisfy the requirements of DSCs. Thereby, all-solid-state nanocomposite electrolyte based on AIIP is prepared in the present study. In this system, iodine, 1,2-dimethyl-3-propylimidazolium iodide (DMPImI), and SiO₂ nanoparticles are added to improve the conduction properties of the electrolyte.

In the DSCs, dye is another key part. As known, ruthenium complexes have exhibited the highest energy conversion efficiency, while metal-free organic dyes have also attracted increasing interest because of their high molar extinction coefficient (ε),[14] diversity of molecule structures, simple synthesis, and low cost.[15,16] Moreover, the higher ε of organic dyes in the visible region allows light harvesting to be accomplished within thinner photoanodes.[14,17,18] Thin TiO₂ films enable a high electron collection ratio,[17,18] making it possible to assemble high-efficiency all-solid-state DSCs. Our group has reported a series of metal-free triphenylamine-based organic dyes.[19–21] Among them, TPAR14 (Figure 1) with rhodanine-3-acetic acid as anchoring group exhibits a considerable efficiency of 6.27% with liquid-state electrolyte.[21] Moreover, for the triphenylamine-based organic dyes, replacement of rhodanine-3-acetic acid by cyanoacrylic acid and appropriate extension of the conjugated system of the dyes can increase the photovoltaic performance.[20,22] Keeping these in mind, a novel triphenylamine-based organic dye of TC15 (Figure 1) is designed and synthesized. The ε of the TPAR14 and TC15 are 39 200 M⁻¹ cm⁻¹ at λ_{max} of 486 nm and 34 100 M⁻¹ cm⁻¹ at λ_{max} of 486 nm (measured in dichloromethane solution, see the Supporting Information for

* To whom correspondence should be addressed. Fax: (86) 22-2350-6808. E-mail: chenabc@nankai.edu.cn.
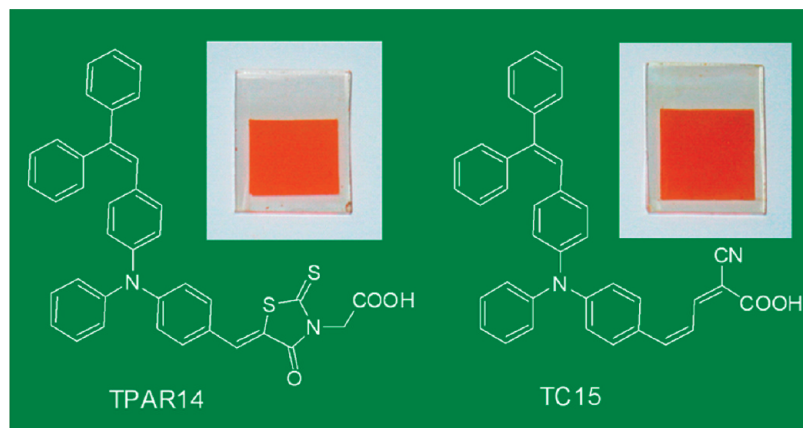
Figure 1. Molecular structures of triphenylamine-based organic dyes of TPAR14 and TC15. The inset photographs are the dye-sensitized TiO$_2$ films.
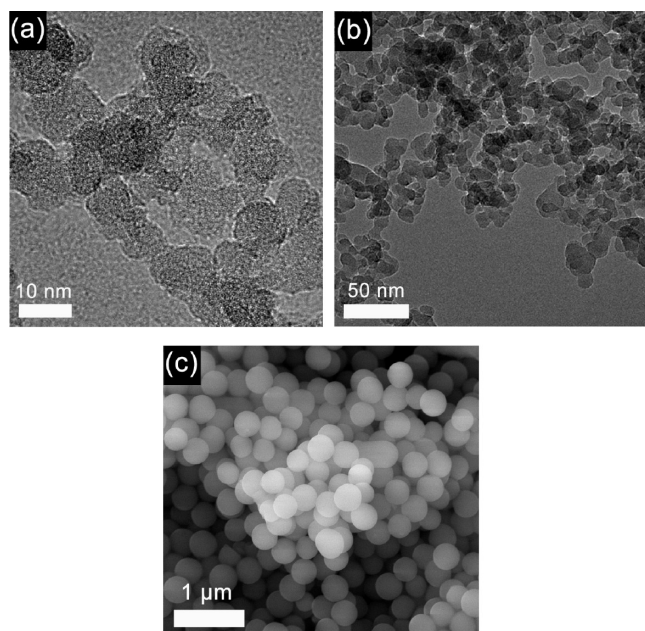

Figure 2. TEM images of SiO$_2$ nanoparticles in sizes of (a) 7−10 and (b) 14−20 nm. SEM image of the SiO$_2$ sample larger than 300 nm (c).

Table S1), which are much higher than that of the ruthenium complexes such as N3 (14 200 M^{-1} cm^{-1} at λ_{max} of 538 nm) and N719 (14 700 M^{-1} cm^{-1} at λ_{max} of 535 nm).[23] It would be valuable to investigate the photovoltaic performance of these two organic dyes combined with all-solid-state electrolyte. Therefore, we report on, for the first time, the preparation and application of AIIP/SiO$_2$ nanocomposite electrolyte to construct all-solid-state DSCs with metal-free organic dyes of TPAR14 and TC15.

Experimental Section

Materials. All reagents used were of analytical grade. Rhodanine-3-acetic acid (Acros) and cyanoacetic acid (Acros) were used as received. SiO$_2$ nanoparticles in sizes of 7−10 (Figure 2a) and 14−20 nm (Figure 2b) were supplied by Degussa AG of Germany. The SiO$_2$ sample larger than 300 nm (Figure 2c) was prepared according to the literature procedure.[24] TiO$_2$ powder (P25, Degussa AG of Germany) consists of 30 wt % rutile and 70 wt % anatase. The conductive glass of fluorine-doped SnO$_2$ (FTO, 20 Ω/sq) was purchased from Wanyelong Company of China. H$_2$PtCl$_6$ was supplied by Shanghai Xingao Chemical Reagent Company. Other reagents were purchased from Jinhua Company of China.

Preparation of All-Solid-State AIIP/SiO$_2$ Nanocomposite Electrolyte. The alkyloxy-imidazolium iodide-based ionic polymer, which was formed by the reaction between 1,1′-(2,2′-oxybis(ethane-2,1-diyl))bis(imidazole) (**1**) and 1-iodo-2-(2-io-doethoxy)ethane (**2**) (Figure 3a),[13] is a white solid power. The fabrication process of the electrolyte is shown in Figure 3b. In a typical preparation, **1** and **2** with molar ratio of 1:1 were dissolved in acetonitrile (MeCN, purified before use). Predetermined amounts of I$_2$, DMPImI, and SiO$_2$ nanoparticles were dispersed in the above solution by ultrasonic method for 5 min. Then, the mixture was heated at 80 °C for 2 h in a closed system to accelerate the polymerization reaction of **1** and **2**. Finally, the reaction system was opened for 24 h to evaporate the MeCN at 85 °C. After that, all-solid-state AIIP/SiO$_2$ nanocomposite electrolyte was obtained (Figure 3c).

Synthesis of Dyes. The organic dye TPAR14 was synthesized based on ref 21. The novel dye TC15 was synthesized in a similar procedure as that for TPAR14. In the final step of the synthesis of TC15, cyanoacetic acid was used in place of rhodanine-3-acetic acid. Recrystallization from ethanol/petroleum ether afforded TC15 as a red solid (73%). For TC15: mp 206−208 °C; ^{1}H NMR (300 MHz, DMSO-d_6) δ 8.05 (d, J = 11.7 Hz, 1H), 7.58−7.51 (m, 3H), 7.20−7.15 (m, 3H), 7.47−7.28 (m, 10H), 7.09−6.95 (m, 6H), 6.88−6.82 (m, 4H); ^{13}C NMR (75 MHz, DMSO-d_6) δ 163.6, 155.6, 149.6, 149.0, 145.7, 144.6, 142.5, 141.0, 140.0, 132.8, 130.6, 130.2, 129.9, 129.6, 129.1, 128.4, 127.8, 127.7, 127.5, 126.9, 125.9, 125.0, 124.1, 120.9, 120.2, 115.5, 102.2; high resolution mass spectral analysis (HRMS) (ESI) for C$_{38}$H$_{26}$N$_2$O$_2$ calcd for [M − H]$^-$ m/z 543.2078, found 543.2073. The absorption, emission, and electrochemical properties of TPAR14 and TC15 dyes are listed inTable S1 of the Supporting Information.

Assembly of DSCs. The FTO glass was washed with ethanol and then immersed in 50 mM TiCl$_4$ aqueous solution at 70 °C for 0.5 h. A layer of TiO$_2$ paste was coated on the pretreated FTO by screen-printing and then dried for 5 min at 125 °C. Figure 4a is a three-dimensional surface image of the TiO$_2$ film prepared by screen-printing one time (about 2 μm, measured by Dektak-150 surface profiler). The thickness of the TiO$_2$ films was controlled by repetition of screen-printing. The prepared TiO$_2$ films were calcined at 450 °C for 30 min. After cooling to room temperature, the films were treated with 50 mM TiCl$_4$ aqueous solution and recalcined at 450 °C for 30 min. The prepared TiO$_2$ film is transparent even by four times screen-
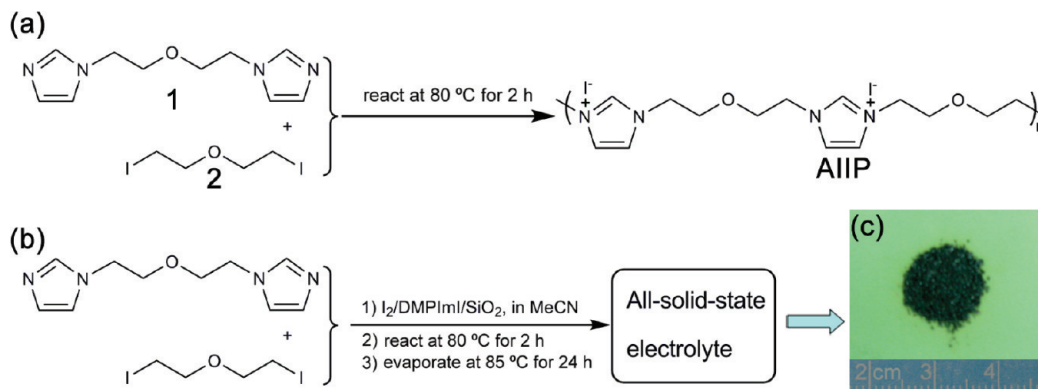
Figure 3. (a) Reaction of 1,1′-(2,2′-oxybis(ethane-2,1-diyl))bis(imidazole) (**1**) and 1-iodo-2-(2-iodoethoxy)ethane (**2**) for the formation of the alkyloxy-imidazolium iodide-based ionic polymer (AIIP). (b) Preparation process of the all-solid-state AIIP/SiO₂ nanocomposite electrolyte. (c) The photograph of the as-prepared electrolyte.
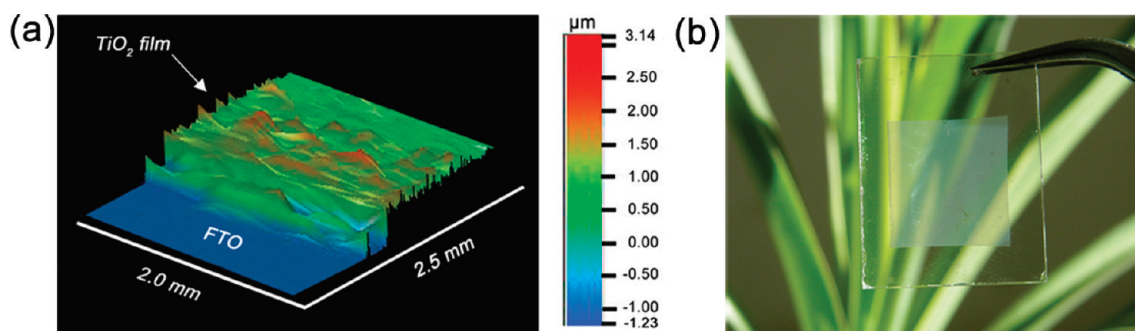

Figure 4. (a) Surface profiling of the TiO₂ film prepared by one time screen-printing and (b) the picture of the transparent TiO₂ film prepared by four times screen-printing.

printing as shown in Figure 4b. Adsorption of the dyes on the TiO₂ surface was done by soaking the TiO₂ electrodes in the dry dichloromethane solutions of TPAR14 and TC15 (standard concentration of 3×10^{-4} M) at room temperature for 24 h in the dark. The photographs of the dye-sensitized TiO₂ films are shown in the inset of Figure 1. The Pt counter electrodes were prepared by spin-coating H₂PtCl₆ solution (50 mM in isopropanol) onto FTO glass and sintering at 390 °C for 0.5 h. The DSCs were made by sandwiching the electrolyte between the dye-covered TiO₂ electrodes and the Pt counter electrodes under pressure.

Instruments and Measurements. The melting point of TC15 was taken on an RY-1 melting point apparatus (Tianfen, China). ¹H and ¹³C NMR spectra were carried out on a Varian Mercury Vx300 MHz spectrometer. HRMS was performed on a high resolution ESI-FTICR mass spectrometer (Varian 7.0 T). The absorption spectra of the dyes in dichloromethane solution and on the TiO₂ film were measured with a Jasco V-550 UV−vis spectrophotometer. The Raman spectra were collected by using an RFS 100/S FT-Raman spectrometer with Nd:YAG laser source and Ge diode detector. FTIR spectra were measured on a FTIR-650 spectrometer (Tianjin Gangdong) at a resolution of 4 cm⁻¹. The thermograms were carried out with a NETZSCH DSC 204 analyzer under Ar atmosphere at a heating rate of 10 deg min⁻¹. The size of the SiO₂ nanoparticles was characterized by SEM (FEI Nova NanoSEM 430) and TEM (Philips Tecnai F20). The interfacial contact between the electrolyte and TiO₂ film was also investigated by SEM.

The ionic conductivity and temperature dependence of the electrolytes were determined by impedance measurements.[13] The conductivity cell, with a structure of platinized FTO/ electrolyte/platinized FTO, was maintained at various con-

stant temperatures for at least 1 h prior to each measurement. Impedance experiments were performed on a computer-controlled PARSTAT 2273 Advanced Electrochemical System (Princeton Applied Research) in the frequency range from 100 kHz to 100 mHz with an amplitude of 10 mV. The open-circuit voltage-decay (OCVD) experiments were also carried out on the PARSTAT 2273 Advanced Electrochemical System.

The photocurrent−voltage (I−V) characteristics of DSCs were measured by a Keithley 2400 digital source meter controlled by a computer. A 500 W xenon lamp served as sunlight simulator in combination with a band-pass filter (400−800 nm) to remove ultraviolet and infrared radiation. Further calibration was carried out by a USB4000 plug-and-play miniature fiber-optic spectrometer (Ocean Co.). The incident-photon-to-electron conversion efficiency (IPCE) can be defined as the ratio of the produced electrons getting across the external circuit ($n_{electrons}$) to the injecting photons ($n_{photons}$). The IPCE values were measured under monochromatic light with 10 nm intervals according to the following equation (eq 1):

$$\text{IPCE}(\lambda) = \frac{n_{electrons(\lambda)}}{n_{photons(\lambda)}} = \frac{1240I(\lambda)}{\lambda\phi(\lambda)} \qquad (1)$$

where $I(\lambda)$ is the current given by the cell at wavelength λ and $\phi(\lambda)$ is the incoming power at wavelength λ. The measurement of IPCE was performed by a similar data collecting system with the above I−V characteristics but under monochromatic light that was obtained by a grating spectrometer (SBP300, Zolix).

All-Solid-State Dye-Sensitized Solar Cells

J. Phys. Chem. C, Vol. 114, No. 14, 2010 **6817**

Results and Discussion

Optimization and Characterization of the Electrolyte. For the low-fluidity electrolyte contained polyiodide species (I_3^-, I_5^-, ... , I_{2n+1}^-), the conductivity mainly depends on (1) the concentration of iodine and (2) the distance between polyiodide species (served as charge transfer centers).[25] This phenomenon can be explained by a mechanism of electrical conduction in polyiodide chains via a Grotthus relay-type mechanism, where a net transport of charge is achieved by electron exchange reaction without any net transport of mass.[25] The conductivity of pure AIIP is less than 10^{-5} mS cm^{-1} because the average distance between I^- ions (>0.7 nm, calculated from bond length and bond angle) is far greater than the radius of I^- ions of 0.22 nm.[25] In this condition, an efficient electron exchange reaction cannot occur. To increase the conductivity with the requirement of DSCs, high-efficiency electron exchange tunnels should be constructed. Thus, I_2, DMPImI, and SiO_2 nanoparticles were added and their contents were optimized step by step to improve the conductivity properties.

Here, I_2 was first introduced into the AIIP. Figure 5a shows the variation of conductivity as a function of mole ratio of iodine to oxygen atoms in the AIIP. Surprisingly, the increase of the ionic conductivity versus the mole ratio of I_2/O does not display a volcano shape but a two-step conductivity dependence. When the mole ratio of I_2/O is less than 0.9, the increase of ionic conductivity is slow. However, when the mole ratio of I_2/O is more than 0.9, the ionic conductivity increases quickly. The results of Raman spectra in Figure 6a reveal that, in the case of the mole ratio of I_2/O less than 0.9, the addition of I_2 to AIIP produces I_3^-. The band at 111 cm^{-1} is ascribed to ν_s of I_3^-.[26] The weak shoulder band at 145 cm^{-1} is probably caused by the ν_a of I_3^-.[26] Due to the larger volume of I_3^- compared with I^-, the Grotthus-type charge transport becomes easier.[25] As a result, the conductivity is gradually improved with increasing the content of I_2. When the mole ratio of I_2/O is more than 0.9, a new peak at 165 cm^{-1} is observed in the Raman spectra, indicating the formation of I_5^- in these systems.[26] Because the volume of I_5^- is even larger than that of I_3^-, the conductivity increases faster in this condition.

The DSCs were fabricated with AIIP incorporating different contents of I_2, and it is found that the optimal energy conversion efficiency was obtained at the mole ratio of I_2/O = 0.9. When the mole ratio of I_2/O is more than 0.9, the photovoltaic performance of the DSCs is reduced by the serious back reaction due to the gradually increased oxidation ability of the electrolytes.[27] Thus, in the following optimization process, the mole ratio of I_2/O is fixed at 0.9.

The solid imidazolium iodide salt DMPImI was added into the above system (with mole ratio of I_2/O at 0.9) to further improve the ionic conductivity. DMPImI, as an additional charge transfer species, is beneficial for the formation of continuous chains of I^- and I_3^- anions. Figure 5b presents the variation of ionic conductivity as a function of the mole ratio of DMPImI to oxygen atoms in the AIIP. As expected, the conductivity is gradually improved as the content of DMPImI is increased. An exciting ionic conductivity of 0.107 mS cm^{-1} is attained at the mole ratio of DMPImI/O = 0.6, which is about 10-fold higher than that without DMPImI (0.0108 mS cm^{-1}). When the mole ratio of DMPImI/O is beyond 0.6, the conductivity decreases, which may result from the aggregates or microcrystallites from excessive DMPImI blocking the transferring of carriers.[25] Thus, the mole ratio of DMPImI/O is fixed at 0.6. We also attempted to replace DMPImI by LiI. However, the conductivity of the
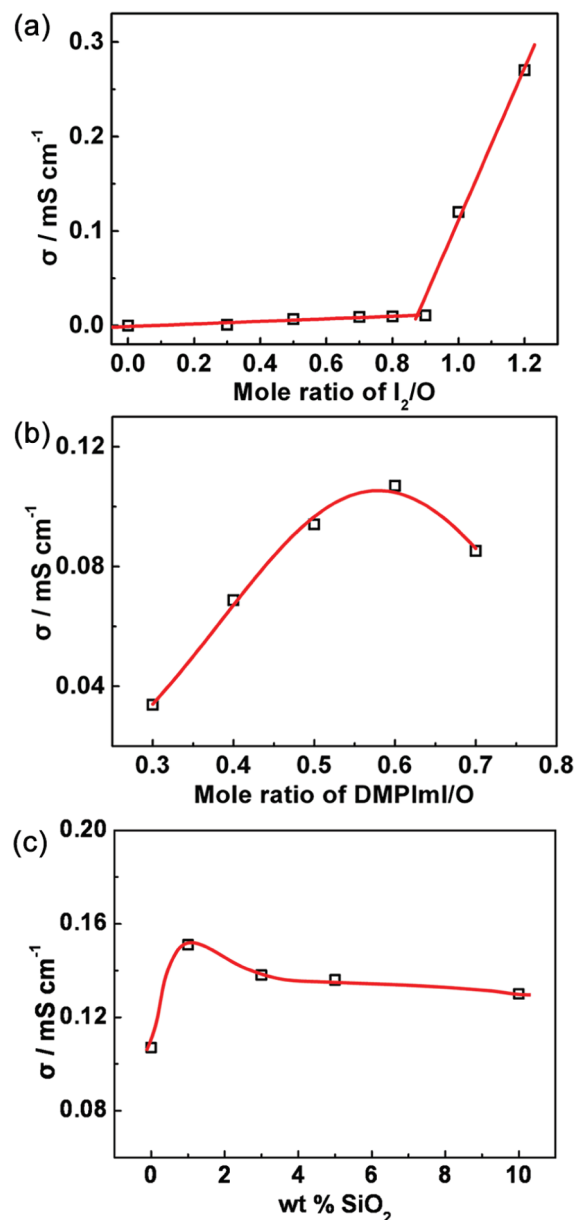

Figure 5. Influence of (a) I_2, (b) DMPImI, and (c) SiO_2 nanoparticles contents on the ionic conductivity of the electrolytes.

electrolyte with LiI is lower than that with DMPImI. This phenomenon is probably caused by the strong interaction between the Li^+ and I^-, which limits the charge transfer.[28]

Finally, the effect of nanoparticles on the ionic conductivity was investigated (Figure 5c). It has been demonstrated that, for the low-fluidity electrolyte contained polyiodide species, the addition of inorganic nanoparticles such as SiO_2 and TiO_2 can increase the ionic conductivity.[29,30] In these nanocomposite electrolytes, the anion species are aligned around the nanoparticles, facilitating the electron exchange reaction.[29,30] It is noted that SiO_2 nanoparticles with the particle size of 7−10 nm are selected because they are sufficiently smaller than the pore diameter of the typical nanoporous TiO_2 layer (10−28 nm).[31] Thereby, the electrolyte can permeate into the TiO_2 layer easily. When 1 wt % of SiO_2 is introduced, the ionic conductivity increases from 0.107 to 0.151 mS cm^{-1}. The added oxide nanoparticles can interact with the oxygen atoms in the polymer through hydroxyl groups on the nanoparticle surface, which is proved by the IR results.
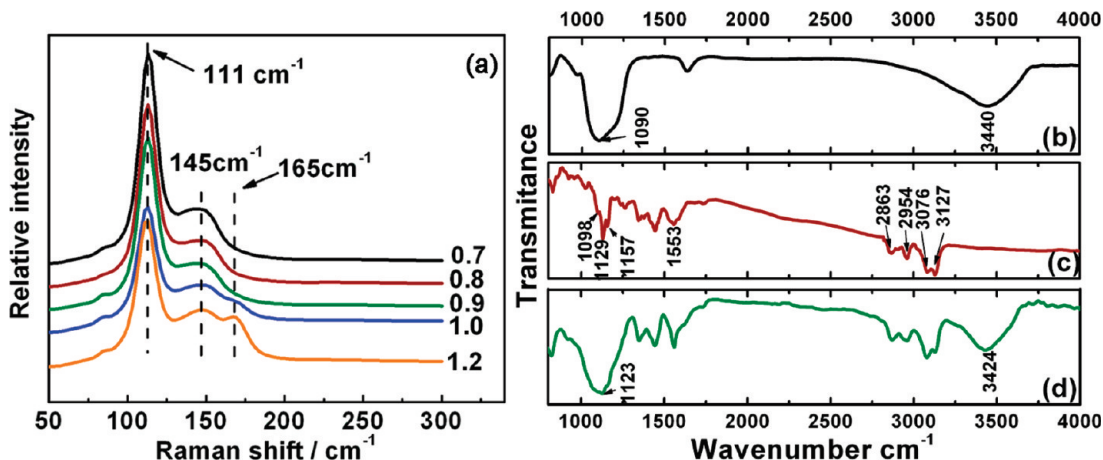
Figure 6. (a) Raman spectra of the electrolytes with different mole ratios of I_2/O (0.7, black; 0.8, red; 0.9, green; 1.0, blue; 1.2, orange). The FT-IR spectra of (b) SiO_2 nanoparticles, (c) electrolyte without SiO_2 (mole ratio of $I_2/O = 0.9$ and DMPImI/O = 0.6), and (d) electrolyte with SiO_2.

Figure 6b shows the FT-IR spectrum of pure SiO_2. The 1090 cm^{-1} peak is assigned to the Si$-$O asymmetric stretching mode. The single peak centered at 3440 cm^{-1} is related to the hydroxyl groups (Si$-$OH) on the surface of SiO_2. Figure 6c displays the FT-IR spectrum of electrolyte without SiO_2 (mole ratio of $I_2/O = 0.9$ and DMPImI/O = 0.6). The peaks at 3127 and 3076 cm^{-1} are caused by the aromatic C$-$H stretching vibrations,[26] while the peaks at 2954 and 2863 cm^{-1} arise from the C$-$H stretching of alkyl. The band at 1553 cm^{-1} is the in-plane C$-$C stretching vibration of the imidazolium ring.[26] Moreover, in Figure 6c, the CN stretching vibrations of MeCN at around 2292 and 2253 cm^{-1} cannot be observed, indicating that the MeCN was evaporated completely from the electrolytes.

When SiO_2 nanoparticles are added, the IR spectrum changes dramatically (Figure 6d). The band related to hydroxyl groups of SiO_2 shifts from 3440 to 3424 cm^{-1}, which is caused by the formation of hydrogen bonds between hydroxyl groups and oxygen atoms in the AIIP. The triplet band of the C$-$O$-$C stretching vibrations becomes a single band with the maximum downshifting from 1129 to 1123 cm^{-1} for the same reason. This phenomenon is also observed for the PEO-based nanocomposite polymer electrolyte.[32] The formation of hydrogen bond interactions makes the AIIP arrange around the SiO_2 nanoparticles, which is very important. The adsorbed AIIP chains are surrounded by continuous chains of I^- and I_3^- anions by

SCHEME 1: Schematic Drawing of the Structure of the AIIP/SiO$_2$ Nanocomposite Electrolyte Containing I$_2$, DMPImI, and SiO$_2$ Nanoparticles
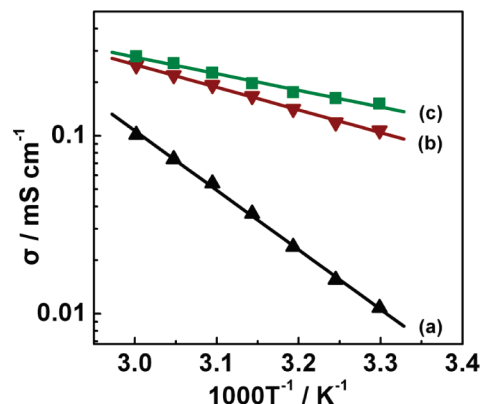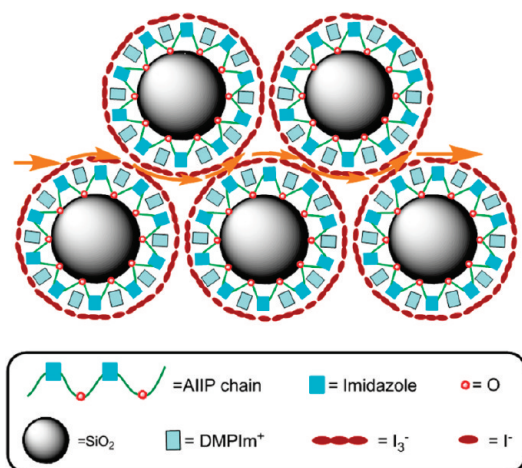

Figure 7. Temperature dependence of ionic conductivity of the electrolytes. The compositions of the three electrolytes are as follows: (a) AIIP and I_2 (mole ratio of $I_2/O = 0.9$, black triangles), (b) AIIP, I_2, and DMPImI (mole ratio of $I_2/O = 0.9$ and DMPImI/O = 0.6, red inverted triangles), and (c) AIIP, I_2, DMPImI, and SiO_2 (mole ratio of $I_2/O = 0.9$, DMPImI/O = 0.6, and 1 wt % SiO_2, green squares).

electrostatic interaction. Thus, high-efficiency electron exchange tunnels with mechanical stability are constructed, which is beneficial to the improvement of conductivity as mentioned above.[29,30]

However, as the SiO_2 content is further increased, the conductivity decreases due to the percolation effect of the nanoparticles.[33] Thus, the optimized electrolyte is composed of I_2 (with mole ratio of $I_2/O = 0.9$), DMPImI (with mole ratio of DMPImI/O = 0.6), and SiO_2 (1 wt %) in AIIP. The structure of the optimal electrolyte is schematically presented in Scheme 1 according to the above analysis.

When larger SiO_2 nanoparticles with the same content were used, such as those with 14$-$20 nm and >300 nm, the conductivity was decreased to 0.142 and 0.116 mS cm^{-1}, respectively. However, these values are still higher than that of electrolyte without SiO_2. These results further proved that the conductivity-enhancement mechanism of the SiO_2 nanoparticles was related to the interfacial interaction.

The temperature dependence of ionic conductivity was also measured to further characterize the conduction properties of the electrolytes (Figure 7). It can be seen that the ionic conductivity increases with temperature because the electron exchange reaction between the charge transfer centers (I^-, I_3^-) becomes faster at higher temperatures. The data in Figure 7 can be fitted well by the following Arrhenius equation (eq 2):

$$\sigma(T) = A \exp\left[\frac{-E_a}{k_B T}\right] \qquad (2)$$

where A is a constant, E_a is the activation energy, k_B is the Boltzmann constant, and T is the absolute temperature.

The E_a of the electrolyte composed of AIIP and I_2 (mole ratio of I_2/O = 0.9, Figure 7a) is calculated to be 64.0 kJ mol^{-1}. Such a high value indicates inferior ionic conduction.[3b] Due to the presence of DMPImI (mole ratio of DMPImI/O = 0.6, Figure 7b), the E_a is obviously reduced (24.4 kJ mol^{-1}). For the optimal electrolyte (Figure 7c), because of the formation of high-efficiency electron exchange tunnels by SiO_2, the E_a is further decreased to 17.9 kJ mol^{-1}, which is even comparable to the reported values of gel electrolytes.[3b,34]

Since the optimal AIIP/SiO_2 nanocomposite electrolyte has the higher ionic conductivity and lower activation energy, the properties of this electrolyte are further characterized in the following. The differential scanning calorimetry analysis (Figure S1, Supporting Information) shows that the melting temperature (T_m) of the electrolyte is 120 °C, which is higher than the previously reported values for other solid polymer electrolytes (around 40−60 °C).[10,11] Apparently, the present electrolyte is in a completely solid state below 120 °C, making it resist higher temperature under continuous irradiation.

For an ideal all-solid-state electrolyte, it should not only have good conductivity but also possess good interfacial contact between the electrolyte and TiO_2 film.[7,11] The poor interfacial contact is the main drawback of the all-solid-state electrolytes which are easy to crystallize.[7,11] The interfacial contact between the electrolyte and TiO_2 film was investigated by SEM. Figure 8 shows the scanning electron micrographs of the cross section of the TiO_2 films before (Figure 8a−c) and after (Figure 8d−f) introducing the AIIP/SiO_2 nanocomposite electrolyte. Panels b and c of Figure 8 display the porous and rough structure of the as-prepared TiO_2 film. After the electrolyte is introduced, the film becomes thicker (Figure 8d). The porous character of the TiO_2 film disappeared even near the FTO because the pores of the TiO_2 film are completely filled with the electrolyte (Figure 8e,f), suggesting a favorable interfacial contact between the electrolyte and the TiO_2 film.

Since this AIIP/SiO_2 nanocomposite electrolyte exhibits favorable conduction and interfacial contact properties, all-solid-state solar cells combined with it and organic dyes are fabricated. Their photovoltaic performance is investigated in the following.

Photovoltaic Performance of All-Solid-State Solar Cells Sensitized by TPAR14 and TC15. It has been demonstrated that, for DSCs with low-fluidity electrolyte, the thickness of the TiO_2 film should be thin (generally ≤8 μm) to permit higher electron collection efficiency.[3,17] However, a thinner TiO_2 film would incur a lower amount of adsorbed dye and limited absorption of incoming light. Organic dyes with a high ε help to compensate for the lower optical incidence depth of the thin photoanode,[17,18] which is beneficial for the application in all-solid-state DSCs. In this study, the TiO_2 film thickness of these all-solid-state solar cells sensitized by organic dyes is optimized to be 8 μm (see Figure S2 in the Supporting Information), which is thinner than the usually used 15 μm for the triphenylamine-based organic dyes combined with liquid-state electrolyte.[19–21]

Figure 9a displays the photocurrent density−voltage (I−V) curves of the all-solid-state solar cell sensitized by TPAR14 (cell A) illuminated at light intensities of 100 and 10 mW cm^{-2}. The corresponding photovoltaic performance parameters of open-circuit voltage (V_{oc}), short-circuit photocurrent density (J_{sc}),
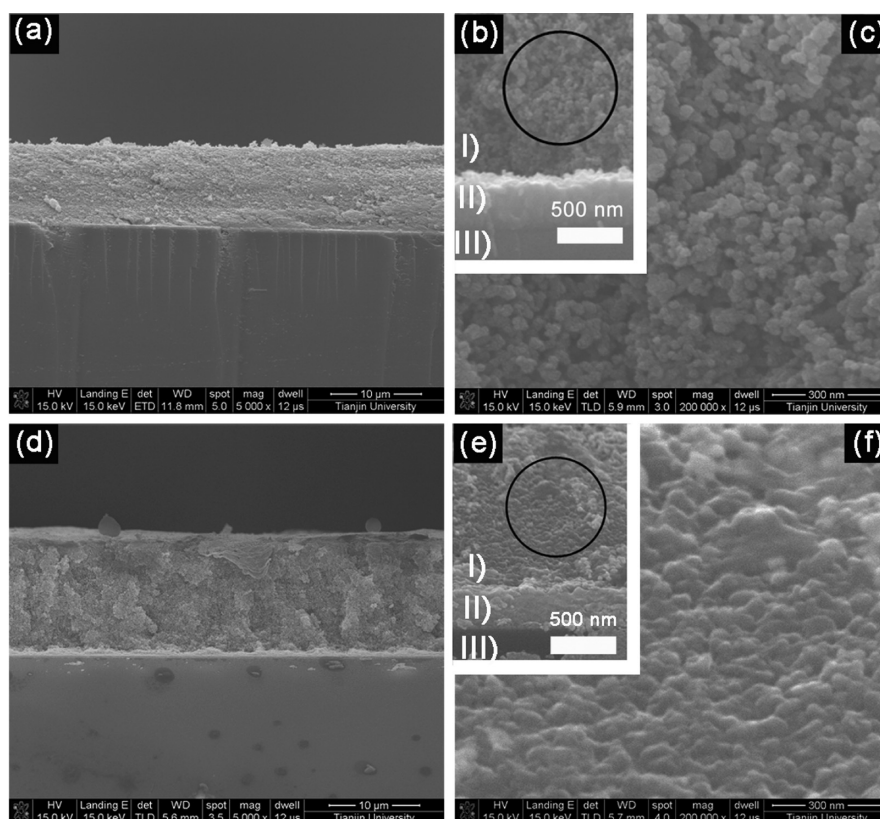

Figure 8. Scanning electron micrographs of the cross section of the TiO_2 films (a−c) before and (d−f) after introducing the AIIP/SiO_2 nanocomposite electrolyte. Panels c and f are magnified parts of panels b and e, respectively. In panel b, layer I is the TiO_2 film, layer II is the FTO, and layer III is the glass; while in panel e, layer I is the TiO_2 film filled with electrolyte, layer II is the FTO, and layer III is the glass.
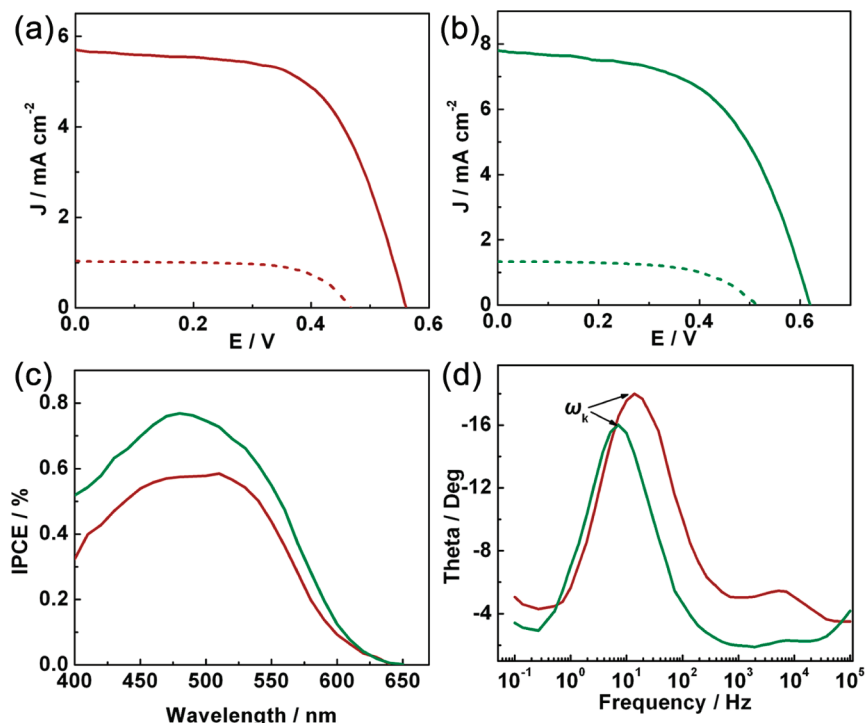
Figure 9. Photocurrent density−voltage curves of (a) cell A and (b) cell B illuminated at light intensities of 100 (solid line) and 10 mW cm^{-2} (dash line). (c) The IPCE spectra of cell A (red line) and cell B (green line). (d) The electrochemical impedance spectra of cell A (red line) and cell B (green line) in the form of Bode plots measured in the dark at a forward bias of −0.62 V.

TABLE 1: Detailed Photovoltaic Performance Parameters of V_{oc}, J_{sc}, FF, and η under Various Light Intensities

cell	light intensity/mW cm^{-2}	V_{oc}/V	J_{sc}/mA cm^{-2}	FF	η/%
A	100	0.561	5.70	0.612	1.96
	10	0.467	1.03	0.664	3.19
B	100	0.619	7.80	0.560	2.70
	10	0.514	1.33	0.602	4.12

fill factor (FF), and η under various light intensities are summarized in Table 1. The illumination intensity has a stronger influence on the performance of the cell because at the lower light level, the photocurrent is small, decreasing the transfer-related losses in J_{sc} and FF and increasing the conversion efficiency.[4,18] Under the illumination intensities of 100 and 10 mW cm^{-2}, the η values of cell A are 1.96% and 3.19%, respectively.

The molecular structure of dye has an important effect on the photovoltaic performance of the DSCs. Generally, the triphenylamine-based organic dyes with rhodanine-3-acetic acid as the anchoring group (TPAR series) exhibit a more serious back reaction than that of dyes with cyanoacrylic acid as the anchoring group (TC series).[22] This serious back reaction, which has relation to the different spatial array of dyes on the TiO$_2$ surface,[22] partly accounts for the lower J_{sc}, V_{oc}, and η of DSCs. In addition, appropriate extension of the conjugated system of the TC dyes is beneficial to the improvement of the η of DSCs.[20] Therefore, a novel triphenylamine-based organic dye (TC15, Figure 1) with cyanoacrylic acid as the anchoring group is designed and synthesized. Moreover, an additional vinyl unit is introduced between the triphenylamine and cyanoacrylic acid in TC15 to extend the conjugated system.

The photovoltaic performance of the TC15 sensitized all-solid-state solar cell (cell B) is shown in Figure 9b. Under the illumination intensity of 100 mW cm^{-2}, the V_{oc}, J_{sc}, and FF of cell B are 0.619 V, 7.80 mA cm^{-2}, and 0.560, yielding an overall

η of 2.70%. An even higher η of 4.12% is obtained upon reducing the lamp intensity to 10 mW cm^{-2}.

As the electrolyte and dye play important roles in the determination of the efficiency of the DSCs, the high η of the all-solid-state solar cell sensitized by TC15 shows that the composition of the electrolyte and the structure of the dye all should be optimized to improve the photovoltaic performance of the DSCs. On the other hand, this high-efficiency AIIP/SiO$_2$ nanocomposite electrolyte can be easily prepared and all the components in it are inexpensive (without the addition of expensive additives such as 4-*tert*-butylpyridine and lithium bis(trifluorosulfonyl)imide), which will further decrease the cost of the DSCs and be beneficial to practical application.

The different photovoltaic performance between TPAR14 and TC15 is simply analyzed here. Figure 9c shows the IPCE of cell A and cell B. The maximum IPCE (76%) for cell B is much higher than that of cell A (58%), which is consistent with the higher J_{sc} of cell B. Electrochemical impend spectra of the two cells were measured to investigate the kinetic process about the back reaction. The Bode plots measured in the dark at a forward bias of −0.62 V are presented in Figure 9d. The peak at intermediate frequencies ($\sim$100−1 Hz) is mainly attributed to the charge transfer at the TiO$_2$/electrolyte interface.[35] The electron lifetime τ can be calculated by the reciprocal of peak frequency ω_k (eq 3):[35]

$$\tau = 1/\omega_k \qquad (3)$$

The τ of cell B is 0.139 s, which is about 2-fold longer than that of cell A with the electron lifetime of 0.072 s. The open-circuit voltage-decay analysis also shows that cell B has a longer electron lifetime than that of cell A (Supporting Information, Figure S3). The longer electron lifetime of cell B contributes to its superior photovoltaic performance. A more detailed

comparison about the different photovoltaic performance of the two dyes by experiments and calculation will be published elsewhere.

Conclusions

All-solid-state DSCs were successfully fabricated by using the AIIP/SiO$_2$ nanocomposite electrolyte and triphenylamine-based organic dyes of TPAR14 and TC15. By optimization of the content of I$_2$, DMPImI, and SiO$_2$ nanoparticles in the electrolyte, considerable ionic conductivity of 0.151 mS cm^{-1} is achieved. The all-solid-state solar cell with this electrolyte and organic dye of TC15 shows a high energy conversion efficiency of 2.70% and 4.12% under the illumination intensities of 100 and 10 mW cm^{-2}, respectively. This type of AIIP/SiO$_2$ nanocomposite electrolyte supplies a new approach to develop low-cost and high-efficiency all-solid-state DSCs.

Supporting Information Available: Absorption, emission, and electrochemical properties of TPAR14 and TC15 dyes, differential scanning calorimetry thermogram of the optimal electrolyte, the correlation between the nanocrystalline TiO$_2$ film thickness and the photovoltaic performance, and open-circuit voltage decays of the DSCs. This material is available free of charge via the Internet at http://pubs.acs.org.

References and Notes

(1) Grätzel, M. *J. Photochem. Photobiol., A* **2004**, *164*, 3.
(2) Wang, P.; Zakeeruddin, S. M.; Moser, J. E.; Nazeeruddin, M. K.; Sekiguchi, T.; Grätzel, M. *Nat. Mater.* **2003**, *2*, 402.
(3) (a) Huo, Z.; Dai, S.; Zhang, C.; Kong, F.; Fang, X.; Guo, L.; Liu, W.; Hu, L.; Pan, X.; Wang, K. *J. Phys. Chem. B* **2008**, *112*, 12927. (b) Shi, J.; Peng, S.; Pei, J.; Liang, Y.; Cheng, F.; Chen, J. *ACS Appl. Mater. Interfaces* **2009**, *1*, 944.
(4) Nogueira, A. F.; Durrant, J. R.; De Paoli, M. A. *Adv. Mater.* **2001**, *13*, 826.
(5) Kumara, G. R. A.; Konno, A.; Shiratsuchi, K.; Tsukahara, J.; Tennakone, K. *Chem. Mater.* **2002**, *14*, 954.
(6) O'Regan, B.; Lenzmann, F.; Muis, R.; Wienke, J. *Chem. Mater.* **2002**, *14*, 5023.
(7) Bach, U.; Lupo, D.; Comte, P.; Moser, J. E.; Weissörtel, F.; Salbeck, J.; Speritzer, H.; Grätzel, M. *Nature* **1998**, *395*, 583.
(8) Johansson, E. M. J.; Karlsson, P. G.; Hedlund, M.; Ryan, D.; Siegbahn, H.; Rensmo, H. *Chem. Mater.* **2007**, *19*, 2071–2078.
(9) Fukuri, N.; Masaki, N.; Kitamura, T.; Wada, Y.; Yanagida, S. *J. Phys. Chem. B* **2006**, *110*, 25251.
(10) Stergiopoulos, T.; Arabatzis, I. M.; Katsaros, G.; Falaras, P. *Nano Lett.* **2002**, *2*, 1259.
(11) Han, H.; Liu, W.; Zhang, J.; Zhao, X. *Adv. Funct. Mater.* **2005**, *15*, 1940.
(12) Bai, Y.; Cao, Y.; Zhang, J.; Wang, M.; Li, R.; Wang, P.; Zakeeruddin, S. M.; Grätzel, M. *Nat. Mater.* **2008**, *7*, 626.
(13) Li, F.; Cheng, F.; Shi, J.; Cai, F.; Liang, M.; Chen, J. *J. Power Sources* **2007**, *165*, 911.
(14) Ardo, S.; Meyer, G. *J. Chem. Soc. Rev.* **2009**, *38*, 115.
(15) Hagberg, D. P.; Edvinsson, T.; Marinado, T.; Boschloo, G.; Hagfeldt, A.; Sun, L. *Chem. Commun.* **2006**, 2245.
(16) Mishra, A.; Fischer, M. K. R.; Bäuerle, P. *Angew. Chem., Int. Ed.* **2009**, *48*, 2474.
(17) Ito, S.; Zakeeruddin, S. M.; Humphry-Baker, R.; Liska, P.; Charvet, R.; Comte, P.; Nazeeruddin, M. K.; Péchy, P.; Takata, M.; Miura, H.; Uchida, S.; Grätzel, M. *Adv. Mater.* **2006**, *18*, 1202.
(18) Kuang, D.; Uchida, S.; Humphry-Baker, R.; Zakeeruddin, S. M.; Grätzel, M. *Angew. Chem., Int. Ed.* **2008**, *47*, 1923.
(19) Liang, M.; Xu, W.; Cai, F.; Chen, P.; Peng, B.; Chen, J.; Li, Z. *J. Phys. Chem. C* **2007**, *111*, 4465.
(20) Xu, W.; Peng, B.; Chen, J.; Liang, M.; Cai, F. *J. Phys. Chem. C* **2008**, *112*, 874.
(21) Pei, J.; Peng, S.; Shi, J.; Liang, Y.; Tao, Z.; Liang, J.; Chen, J. *J. Power Sources* **2009**, *187*, 620.
(22) Tian, H.; Yang, X.; Chen, R.; Zhang, R.; Hagfeldt, A.; Sun, L. *J. Phys. Chem. C* **2008**, *112*, 11023.
(23) Nazeeruddin, M. K.; Zakeeruddin, S. M.; Humphry-Baker, R.; Jirousek, M.; Liska, P.; Vlachopoulos, N.; Shklover, V.; Fischer, C.-H.; Grätzel, M. *Inorg. Chem.* **1999**, *38*, 6298.
(24) Stöber, W.; Fink, A.; Bohn, E. *J. Colloid Interface Sci.* **1968**, *26*, 62.
(25) Wu, J.; Hao, S.; Lan, Z.; Lin, J.; Huang, M.; Huang, Y.; Li, P.; Yin, S.; Sato, T. *J. Am. Chem. Soc.* **2008**, *130*, 11568.
(26) Jerman, I.; Jovanovski, V.; Vuk, A. Š.; Hočevar, S. B.; Gaberšček, M.; Jesih, A.; Orel, B. *Electrochim. Acta* **2008**, *53*, 2281.
(27) Wang, H.; Liu, X.; Wang, Z.; Li, H.; Li, D.; Meng, Q.; Chen, L. *J. Phys. Chem. B* **2006**, *110*, 5970.
(28) Bhattacharya, B.; Lee, J. Y.; Geng, J.; Jung, H.-T.; Park, J.-K. *Langmuir* **2009**, *25*, 3276.
(29) Berginc, M.; Hočevar, M.; Krašovec, U. O.; Hinsch, A.; Sastrawan, R.; Topič, M. *Thin Solid Films* **2008**, *516*, 4645.
(30) Kang, M.-S.; Ahn, K.-S.; Lee, J.-W. *J. Power Sources* **2008**, *180*, 896.
(31) Hu, L.; Dai, S.; Weng, J.; Xiao, S.; Sui, Y.; Huang, Y.; Chen, S.; Kong, F.; Pan, X.; Liang, L.; Wang, K. *J. Phys. Chem. B* **2007**, *111*, 358–362.
(32) Xiong, H.; Zhao, X.; Chen, J. *J. Phys. Chem. B* **2001**, *105*, 10169.
(33) Wang, H.; Li, H.; Xue, B.; Wang, Z.; Meng, Q.; Chen, L. *J. Am. Chem. Soc.* **2005**, *127*, 6394.
(34) Choe, H. S.; Carroll, B. G.; Pasquariello, D. M.; Abraham, K. M. *Chem. Mater.* **1997**, *9*, 369.
(35) Adachi, M.; Sakamoto, M.; Jiu, J.; Ogata, Y.; Isoda, S. *J. Phys. Chem. B* **2006**, *110*, 13872.